Journal of Energy Storage 72 (2023) 108621

Contents lists available at ScienceDirect

Journal of Energy Storage

journal homepage: www.elsevier.com/locate/est

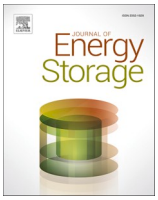

Research papers

Control method to coordinate inverters and batteries for power ramp-rate control in large PV plants: Minimizing energy losses and battery charging stress

A. González-Moreno [a,*], J. Marcos [a,b], I. de la Parra [a,b], L. Marroyo [a,b]

[a] Department of Electrical, Electronic and Communications Engineering, Public University of Navarra, 31006 Pamplona, Spain
[b] Institute of Smart Cities (ISC), Public University of Navarra, 31006 Pamplona, Spain

ARTICLE INFO

Keywords:
Inverter limitation
Battery energy storage system (BESS)
PV smoothing
PV-battery integration

ABSTRACT

This work presents a novel control method for multi-megawatt photovoltaic (PV) plants that is able to regulate each plant inverter and the battery system to mitigate PV power fluctuations. The proposed control method makes it possible to implement different PV ramp-rate control strategies based on the use of batteries and the limitation of inverters during positive fluctuations, which have been conceptually proposed in the specialized bibliography, but have omitted how to perform the coordination between PV generators. The dynamic model and the tuning of the control parameters are presented and the method is used to correctly implement different inverter-limitation strategies using 5-second data from a real 45 MWp PV plant. Furthermore, a new control strategy is proposed. This strategy reduces curtailment losses to negligible values and takes into account and addresses the intrinsic asymmetry in the battery charging and discharging capability, an issue that has been overlooked in the specialized bibliography. The results show that the proposed control method can effectively control each of the multiple inverters in order to obtain the desired PV plant operation to regulate the battery charging power, even during highly fluctuating scenarios.

1. Introduction

Nowadays, photovoltaic (PV) power is one of the generation technologies with the lowest levelized cost of energy (LCOE) [1–3]. Consequently, and due to the urgent need to reduce greenhouse emissions, the worldwide PV generation capacity has dramatically increased over the last few years [4,5]. Despite the benefits of this extraordinary growth in PV installations, this situation can also challenge the quality and stability of the power grid: the intrinsic intermittency of the solar resource and the increase in the proportion of power electronic-based generators to the detriment of synchronous ones (thereby reducing the inertia of the electrical system). The potential concerns associated with severe PV power fluctuations, particularly in scenarios of weak grids or high PV penetration, are voltage fluctuations [6,7] and frequency deviations [8,9]. These concerns have led some transmission system operators (TSO) to request ramp-rate limitations on power dispatched from PV and other renewable sources (Puerto Rico [10], Ireland [11], China [12], Denmark [13], Australia [14] or South Africa [15], among others).

In order to meet these requirements, PV projects must deal with the excess or lack of energy caused by power fluctuations. A number of strategies have been proposed [16], the vast majority of which require energy storage systems (ESS), mainly Lithium-ion batteries, to maintain the dispatched power within the required limits. The algorithm that controls the charge and discharge process plays a preponderant role, not only on the size of the battery needed but also on the way in which the battery is used and, therefore, on its life expectancy. Hence, this control strategy is essential in order to minimize the additional cost incurred by the use of batteries and to limit the loss of competitiveness in the PV LCOE.

Initially, different types of low-pass filters were proposed, for example: moving average or first and second order filters [16,17]. In these cases, the dispatched grid power (P_g) is easily obtained by applying the selected filter to the PV power signal (P_{pv}). The battery power is calculated as the difference between P_{pv} and P_g. In general terms, this family of strategies injects the mean value of the PV power during a preset time window, introducing a delay. Consequently, the storage equipment permanently cycles regardless of whether or not there is a PV fluctuation, producing at least one deep cycle per day. This kind of

* Corresponding author.
E-mail address: alejandro.gonzalez@unavarra.es (A. González-Moreno).

https://doi.org/10.1016/j.est.2023.108621
Received 16 March 2023; Received in revised form 31 July 2023; Accepted 3 August 2023
Available online 27 August 2023

approach would produce over-smoothing at the expense of increased ESS energy throughout [18,19], which not only implies higher losses but also accelerates the degradation of an expensive and critical item of equipment such as the battery. In order to reduce battery cycling advanced filters have been proposed that would reduce the delay introduced by the filter, such as hull enhanced linear exponential smoothing (HELES) [20], however, these strategies do not completely eliminate the delay, the over attenuation and, therefore, a degree of unnecessary cycling.

As an alternative to these methods, classic ramp-rate control strategy was proposed. The intention is to use the battery only when needed. This strategy sets a limit to the grid power, by controlling the battery power, only if the rate of change of P_{pv} exceeds the ramp-rate limit requested by the TSO (r) and then to restore the battery setpoint [21,22]. In this way, the battery is just used when needed, and battery degradation is reduced by up to 10 times [21]. However, due to the fact that the sign of the next fluctuation is unknown, the ESS must at all times have the capacity to absorb/dispatch the energy corresponding to the worst possible upward or downward fluctuation that could occur [21]. Therefore, a state of charge (SOC) control is required with the reference set at 50 % and a minimum capacity that is twice as high as the energy associated with the worst-case fluctuation [21]. However, despite the fact that the classic ramp-rate control makes a non intensive usage of the battery, it also requires, for the same ramp-rate attenuation, at least twice as much storage compared to filter-based methods [21].

In an effort to enhance the performance of the classic ramp-rate control, a new strategy was proposed [23], named clear sky-dark sky ramp-rate control. While it is true that the sign of the next fluctuation is unknown in advance, the power limits of the plant are known and the maximum positive and negative power fluctuations can be estimated at each instant [23]. Thus, this strategy implements a variable SOC reference that guarantees the ability to smooth both these fluctuations, making possible to work with minimum battery capacity, which is the one needed to smooth the worst-case fluctuation at a PV plant (the concept is explained in Section 3). As a trade-off for the reduction in battery size, the clear sky-dark sky strategy increases the cycling, compared to classic ramp-rate control, by up to 3 times [23].

As an alternative to the use of ESS, which is mandatory in both ramp-rate control and filter-based strategies, it has been proposed to limit inverters to smooth PV generation [24,25]. If the inverters are set so that they do not operate at maximum power point tracking (MPPT), any power surge can be mitigated when clouds leave the plant by limiting part of the energy. As this method does not require ESS, just software modifications, its cost of implementation is particularly low [24]. However, this approach is not able to smooth out downward fluctuations since, without ESS, it is not possible to compensate for the lack of power when clouds block the Sun.

If ramp-rate control is combined with inverter limitation, it is possible to smooth both upward and downward fluctuation. A number of studies have proposed methods that combine ramp-rate control strategies with inverter curtailment in large PV plants [23,26–29]. The operating principle is to limit any positive fluctuation by forcing inverters to operate outside their maximum power point tracking (MPPT) and to smooth downward fluctuations using the battery. As the battery is only required to mitigate negative fluctuations, battery cycling could be reduced to values close to the classic ramp-rate control [23]. Evidently, the main disadvantage of these methods is the energy losses associated with the intrinsic power curtailment. Specifically, in [23] the curtailment of the generation of each PV inverter (P_{inv}) was proposed for any instant in which its power increases faster than the maximum allowed ramp-rate (r). However, the solution is implemented in each inverter independently and does not take advantage of the smoothing effect produced by the geographical distribution of PV generators [30,31]. Consequently, considerable annual production losses would appear, e.g. 9.09 % of the total production at a plant with a peak power of 45 MW and a ramp-rate restriction of 2 %/min [23].

It has been demonstrated, at a concept level, that the losses can be reduced firstly by limiting the increase of the PV plant power to the maximum allowed ramp-rate instead of the individual inverter power [26] and secondly by postponing the inverter limitation when a positive fluctuation takes place and the battery is not fully charged [27,29]. For the same ramp-rate constraint (2 %/min), and facilities with a peak power of 45 and 10 MW, the annual losses are reduced to 2.33 % [26] and 3.27 % [27], respectively. In [29] the authors were able to reduce the annual limitation losses below 1 % by applying a variable gain in the battery control loop, which would avoid charging the battery at low irradiances. However, a major drawback of the proposals that combine ramp-rate control and inverter-limitation is that none of them address how to implement the coordination between the inverters, which is mandatory in order to control the ramping of the entire plant in the way they propose. This coordination is especially difficult to implement because it needs to be very precise in conditions of high variability in the operating point of each of the multiple PV plant inverters. In other words, although [26,27,29] propose strategies at a concept level, they do not developed a control method capable of performing the constraint of multiple PV inverters in a coordinated manner. In fact, the simulations were done as if the multi-megawatt plants (45 and 10 MWp) were made of a single inverter. In addition, and like any of the current strategies, the asymmetric damage to the battery caused by the charging and discharging process is not taken into account, particularly in [27,29]. This last issue has already been highlighted in [28], but their proposed solution was only tested on one inverter and no method was developed to apply it to a large-scale plant with multiple PV generators.

This paper propose a new control method that is able to control in a coordinated manner the operating point of each of the multiple PV plant inverters during highly fluctuating scenarios and all of them with the battery system. As far as we are aware, this is the first proposal of its kind. Although a communication system is required to implement this control method, it will be shown that the system communication currently used in photovoltaic plants is sufficient. Secondly, a new control strategy is proposed which, using the proposed control method, is able to reduce the energy wastage to insignificant values. Furthermore, the control strategy can operate with batteries with an asymmetric charge and discharge power capability, as it ensures that the battery does not charge at high power rates (avoiding unnecessary degradation). Finally, like any other inverter-based strategy, it can function with minimum storage requirements.

The study is organized as follows: Section 2 describes the origin and type of data used; Section 3 briefly explains the worst-case fluctuation concept and relates it to the minimum storage requirement, as a function of the desired ramp-rate limitation and plant size. Section 4 explains the system operation and limitations of the non-coordinated strategy and Section 5 explains the proposed control method to perform coordinated inverter-limitation, in particular the control loop that makes it possible, from its concept to its flexibility to perform different limitation strategies (including a novel one). Section 6 presents the simulation results of all the inverter limitation strategies using the proposed algorithm and their performance in the short and long-term. Finally, Section 7 presents the conclusions of the study.

2. Experimental data

Over a one-year period, data were recorded at the Amareleja PV plant (Fig. 1(a)) in southern Portugal (38°11′20″N, 07°12′08″0W). The 250-hectare PV plant consists of 2520 vertical solar trackers, with a tilt angle of 45° and a ground cover ratio (GCR) of 0.162. Each group of 36 solar trackers are grouped together and connected to a 550 kW DC/AC inverter. With a total number of 70 inverters, the plant peak power is 45.6 MW while the inverter rated power (P_N) is 38.6 MW.

The synchronized series of each inverter were obtained with a 5-second sampling period. In post-processing, the series for the 70 inverters were grouped into pairs to obtain data with a nameplate capacity of 1.1

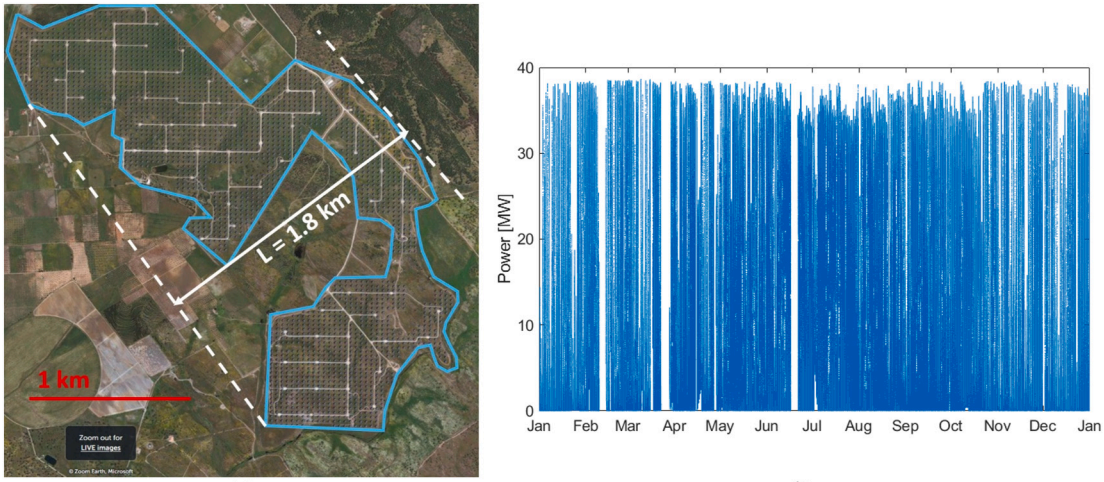

(a) (b)

Fig. 1. Amareleja PV plant in southern Portugal (38°11′20″ N,7°12′8″ W). (a) Layout and shortest dimension, L. (b) 1-year 5-second sampled plant PV power series.

MW, which is currently more realistic than the original 550 kW, and to reduce the computational effort during simulation. In this way, the PV plant analyzed would consist of 35 equivalent inverters.

3. Minimum storage

The value of the minimum battery capacity required to ensure the correct operation of any inverter limitation-based strategy is intrinsically related to the worst-case possible fluctuation, which could occur in central daytime when a rapid cloud front covers (or leaves) the PV plant following the direction of its shortest dimension (L). For Amareleja PV plant L is shown in Fig. 1(a). The shape of the worst-case power fluctuation has been described and fitted by an exponential decay with time constant τ [22] (see Fig. 2), which depends on L. The equation, with power in pu, that approximates the worst negative fluctuation is given by (1):

$$P_{pv} = \Delta P_{max} \cdot e^{-t/\tau} + (1 - \Delta P_{max}) \tag{1}$$

where ΔP_{max} is the total power variation that occurs when a clear sky is followed by a fully overcast one and, consequently, the power source changes from primarily direct to uniquely diffuse radiation. In this work, based on our data (Fig. 1(b)), we used a minimum diffuse power of 5 % ($\Delta P_{max} = 0.95$). The time constant of (1) can be approximated as (2) [22]:

$$\tau[s] = 42L[km] - 0.55 \tag{2}$$

Then, the amount of energy to smooth the worst fluctuation (E_{wf}), with a specific ramp-rate restriction (r), is obtained with the integration of the region between (2) and a straight line with slope r [22], as is exemplified in Fig. 2. The analytical result of the integral is (3), with power expressed in pu:

$$E_{wf} = \Delta P_{max}\left(\frac{\Delta P_{max}}{2r} - \tau\right) \tag{3}$$

The energy described by (3) is the minimum usable storage to be able to smooth any possible fluctuation. In (3) the units must be coherent, e.g. the time units of r and τ must be the same, as well as the power units of r and ΔP_{max}.

In this study, the total capacity (C_b) was oversized compared to the minimum value obtained from (3), which is a common practice in real applications. Additionally, no discharge was allowed when the state of charge reached 20 %. The remaining 80 % is equal to E_{wf}, which means that the applied oversizing was 25 %:

$$C_b = \frac{1}{0.8} E_{wf} = 1.25\, E_{wf} \tag{4}$$

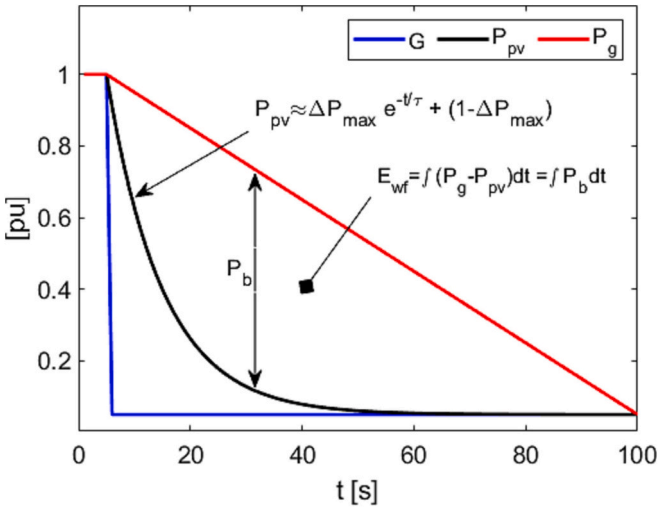

Fig. 2. Worst fluctuation model. G: Irradiance at a single point, P_{pv}: PV power, P_g: injected grid power with ramp-rate compliance.

4. Ramp-rate limitation using non-coordinated inverters

In the case of non-coordinated inverters (hereinafter Strategy 0), to ensure the positive ramps of the PV plant do not exceed the maximum allowed ramp-rate (r), the inverters are programmed to limit their ramp-up to r ($\Delta P_{inv,i} \leq r$) [23]. The Battery System smooths the negative PV fluctuations by injecting power to maintain $P_g \geq -r$ and recharges the battery afterwards.

The control diagram of Strategy 0 is represented in Fig. 3. Its general operation is as follows: the sum of each inverter power output is the limited plant power (P_{lim}), which can be equal to or less than the available power (P_{pv}), depending on whether there is inverter limitation or not. The reference of the grid power (P_g^*) is obtained as the difference between P_{lim} and the proportional action of the storage control loop (P_Δ). This reference is fed into a ramp-rate limiter to ensure that the grid power will meet the ramp-rate restriction, even after the SOC control action, thus obtaining the damped power to be sent to the grid (P_g). The difference between P_g and P_{lim} must be injected/absorbed by the battery (P_b) and its integration (considering the battery efficiency η_b and total capacity C_b) is the normalized stored energy (E_b), which was used as SOC

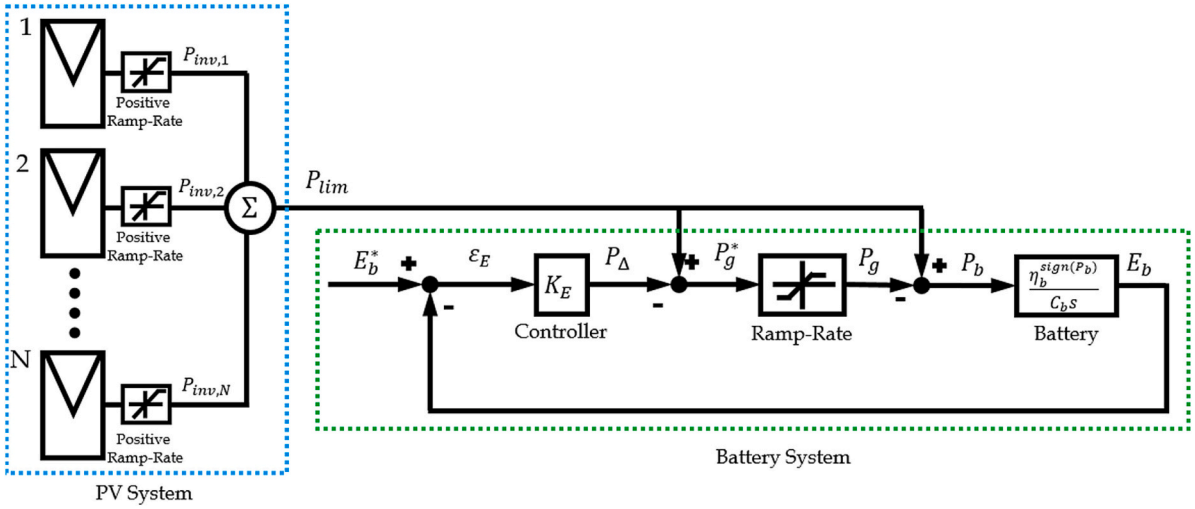

Fig. 3. Stored energy control diagram of the ramp-rate limitation with inverters (Strategy 0).

approximation (5):

$$SOC \approx E_b = \frac{\eta_b^{sign(P_b)} P_b}{s \cdot C_b} \tag{5}$$

Battery efficiency was considered to be constant but not symmetric, it was assumed to be 90 % in charge and 95 % in discharge, the total capacity was obtained from (4) (see Table 1 for the required capacity for different ramp-rate restrictions).

Finally, E_b is compared to the reference (E_b^*) to produce the proportional control action (P_Δ). According to [23], E_b^* should be set to 100 % in order to be able to mitigate the worst-case negative fluctuation at any time.

This approach achieves two main benefits: firstly, any strategy based on inverter limitation is able to function with minimum storage [23,26], minimizing the additional investment to smooth PV power (price of the battery). Secondly, compared to other minimum storage strategies [23], the use of the battery is reduced given that it is not fully required in positive power transitions, thereby extending the battery lifespan [23].

However, Strategy 0 involves large limitation losses that would have a negative financial impact on a project. As an example, two limiting scenarios are shown in Fig. 4, where the evolution of each inverter during two different kinds of fluctuation can be observed (gray lines). The first case (Fig. 4(a)) shows the smoothing of a severe positive fluctuation, with r=10 %/min; the second one (Fig. 4(b)) shows how the strategy performs when a sharp downward fluctuation is immediately followed by an upward one, with $r = 2$ %/min. In both cases, the wasted production can be observed by comparing the difference between the available PV power (black-dotted line) and the limited power (red line). For this particular day (28th of January) the limitation losses are as high as 32 % and 8.9 %, for $r = 2$ %/min and $r = 10$ %/min, respectively.

The large curtailment losses are mainly due to the lack of coordination between the different elements of the system (see Fig. 3). On the one hand, due to the non-coordination of the inverters (Fig. 4(a)), given that P_{lim} is the sum of the power of each inverter (N in total), the plant power increase would be equal to r only when all inverters are being limited at the same time, and less than r otherwise. As a result, at the beginning of the fluctuation, when few inverters are being limited, the growth of P_{lim} is slower than the ideal one (yellow-dashed line), which delays the instant when the total ramp rate of the plant reaches r. This over-limitation can be observed in the difference between ideal and actual limited power (red line). This type of over-curtailment losses would have a considerable impact when the ramp-rate restriction is not particularly demanding (such as $r = 10$ %/min).

In the second case (Fig. 4(b)), due to the lack of coordination between the inverters and the battery control loop, the increase in P_{lim} is at most r, even if it is directly undesirable. As can be seen, when an upward fluctuation immediately follows a deep downward one (at 10:26), then the uncoordinated limitation becomes particularly counterproductive: since if P_{lim} is below P_g, the battery is being severely discharged and, at the same time, the inverters are being limited. This contradictory operation, in which energy is simultaneously required and wasted, produces considerable curtailment losses, increases battery semi-cycle depths and unnecessarily prolongs discharge at higher power/current rates. Contrary to the previous over-limitation mechanism, this one would have a considerable impact when the ramp-rate restriction is demanding (such as $r = 2$ %/min).

Furthermore, a third mechanism of avoidable curtailment losses can be observed in the previous two cases. During the upward fluctuation of a plant, some inverters may suddenly be covered by a cloud which would reduce their production. Given that the remaining inverters do not offset this sudden drop, P_{lim} not only reduces its slope, but also may even suffer a transitory negative ramp-rate. This can be observed after 12:46 and 10:35 in Fig.4(a) and (b), respectively.

In order to avoid this kind of unnecessary limitation, the local limiting value of inverters should take account of plant-level variables, such as P_{lim} or P_g, and not just local ones. This can be done if the communication existing between inverters and the plant controller is used.

Table 1
Battery sizing for inverter-limitation strategies depending on different simulated ramp-rate restrictions (r).

r [%/min]	C_b [MWh]	C_b/P_N [min]
1	35.3	54.9
2	17.2	26.7
5	6.3	9.8
8	3.6	5.5
10	2.6	4.1

5. Proposed control method to coordinate inverter limitation

It has been demonstrated that the individual limitation of the inverters (Strategy 0) does not take advantage of the smoothing of the fluctuations produced by the geographical distribution of the PV generators and limits the PV power when this is not necessary (as can be seen in Fig. 4), so significant limitation losses occur. However, it is not clear how to control P_{lim} when there is a high variability in the operating point of the PV generators and their derivative. Although [26,27]

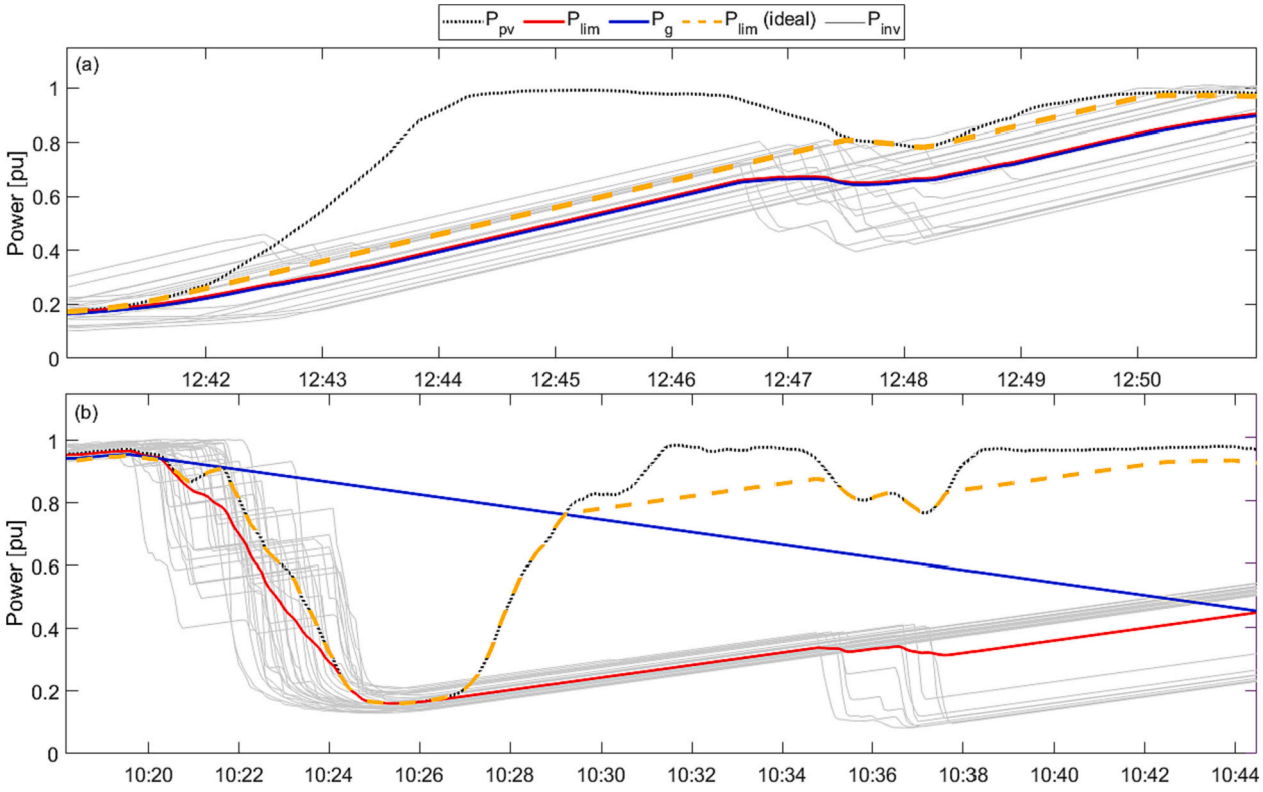

Fig. 4. Strategy 0 behavior during portions of 28th of January. (a) $r = 10$ %/min and (b) $r = 2$ %/min. Available PV power P_{pv} (black-dotted), limited PV power P_{lim} (red), injected power P_g (blue), ideal P_{lim} (yellow-dashed) and inverters' production P_{inv} (gray). (For interpretation of the references to colour in this figure legend, the reader is referred to the web version of this article.)

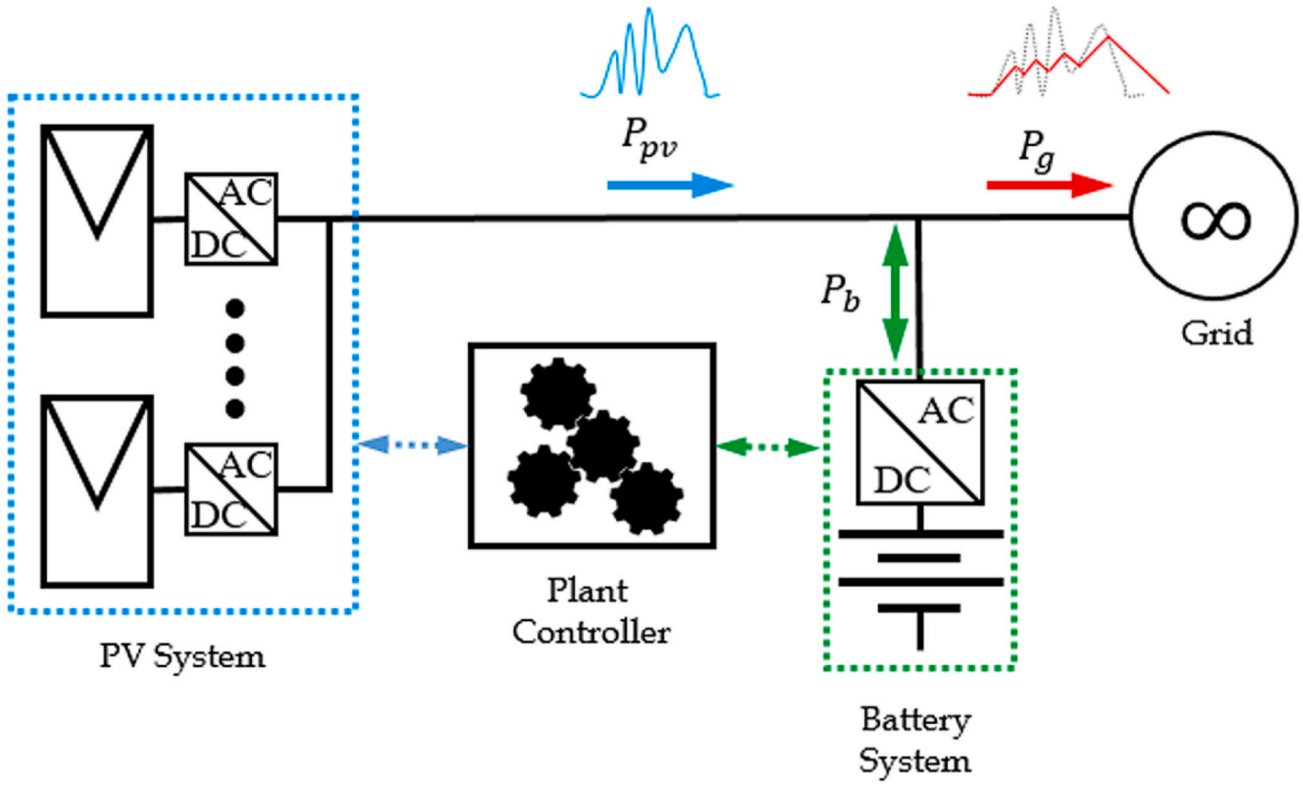

Fig. 5. Schematic diagram of a multi-megawatt PV plant with battery storage and smoothing capabilities connected to the grid.

propose strategy concepts for coordinated inverters, no algorithm capable of performing the constraint of multiple PV generators in a coordinated manner is proposed. In fact, the simulations were done assuming that the plant was a single inverter.

However, any PV plant with ramp-rate limitation capabilities can be conceptualized as in Fig. 5, where three subsystems can be abstracted. First, the PV System (inverters and PV modules) generates fluctuating power (P_{pv}); second, the Battery System injects or absorbs power (P_b) to maintain the variation of dispatched grid power (P_g) within the required limits; finally, the Plant Controller, which performs the normal actions such as SCADA, reactive power control, responding to TSO requirements, etc., and could also be used to coordinate the previous two.

To modify the PV plant operating point in a desirable way, each inverter power ramp-rate needs to be regulated with a central algorithm. The aim of the proposed control method is to be able to coordinate all the inverters at the PV plant and also them with the storage system during the entire operation. To do so, a new control loop, named *Smart Limitation Loop* (SLL) is implemented in the plant controller. SLL calculates the maximum allowed increase (r^*_{max}) for all the inverters and the SOC reference E^*_b for the battery subsystem (see Fig. 6). The PV System and the battery control loop are similar to those shown in Fig. 4, but the references (r^*_{max} and E^*_b) are constantly calculated and transmitted from the Plant Controller.

5.1. Smart Limitation Loop (SLL) design

The Plant Controller collects the values of interest (P_{lim}, P_b, P_g, E_b and r) and generates the proper references (E^*_b and r^*_{max}). The key factor in the coordination of the PV inverters is SLL (Fig. 7), which is responsible for regulating the limited PV power and for allowing the indirect control of the battery power during upward power fluctuations. The performance of the plant is easier to analyze if it is represented in the discrete domain and in pu, with the nominal plant and individual inverter power as the bases at plant and inverter level.

SLL has the flexibility to implement different limitation strategies depending on the value of the battery power reference (P^*_b). The limited PV power reference (P^*_{lim}), which is used as the reference of the feedback loop, is the sum of P_g and P^*_b. The controller produces a unique maximum increase for all the inverters (r^*_{max}), instead of sending a specific reference for each one. In order to avoid undesirable curtailments, r^*_{max} is limited if it is less than r_{min}, a minimum value that depends on the strategy (see below). The PV inverters will be locally limited according to the transmitted reference. Therefore, if an inverter varies with a rate lower than r^*_{max} it will not be limited, and only those that would vary at higher rates will be curtailed. From the point of view of a single inverter, the above can be described as follows:

$$P_{inv,i}(k) = min\left\{P_{inv,i}(k-1) + r^*_{max}\,(k-1)\,, P_{MPPT,i}(k)\right\} \tag{6}$$

where $P_{inv,i}$ and $P_{MPPT,i}$ denote the instantaneous and the MPPT algorithm power of the i-th inverter, respectively.

The reference of SLL (P^*_{lim}) is designed to avoid excessive curtailment losses, as those exemplified in Fig. 4(b). First of all, P^*_b would always be positive, then P^*_{lim} is always higher than P_g. As a result, when P_g is higher than P_{lim}, the loop error ($\varepsilon_{lim} = P_g + P^*_b - P_{lim}$) and, consequently, r^*_{max} would be high; hence, following (6), no limitation would be applied. Only when ε_{lim} is small enough r^*_{max} would have an effect on P_{lim}. In this condition, if r^*_{max} is applied to each of the inverters, the total power plant increase would be (7):

$$\Delta P_{lim}(k) = r^*_{max}(k-1)\cdot\frac{N_{eff}}{N}(k) \tag{7}$$

where N is the total number of inverters, 35 in this work, and N_{eff} is a quantity representing a hypothetical number of inverters whose power increases at r^*_{max} with the same effect as all the N inverters increasing with different rates (some at r^*_{max} and others at lower values). To be clear, at the beginning of any severe positive power fluctuation a few inverters start to increase before the rest, as in Fig. 4(a), and they are the first to be limited, in the limit just one is ($N_{eff} = 1$). On the other hand, in the middle of the fluctuation, most of the inverters are experiencing severe power fluctuations (most of them need to be curtailed), in the limit all of them are ($N_{eff} = N$). Finally, at the end of the event, only a few inverters need to be limited, the last ones that start to change, and the effect is the same as at the beginning of the fluctuation, but with different inverters being curtailed.

As will be seen, the communication delays, two in the feedback loop and one in the measurement of P_g (see Fig. 7), have no significant impact on the performance of the algorithm and it can operate correctly with

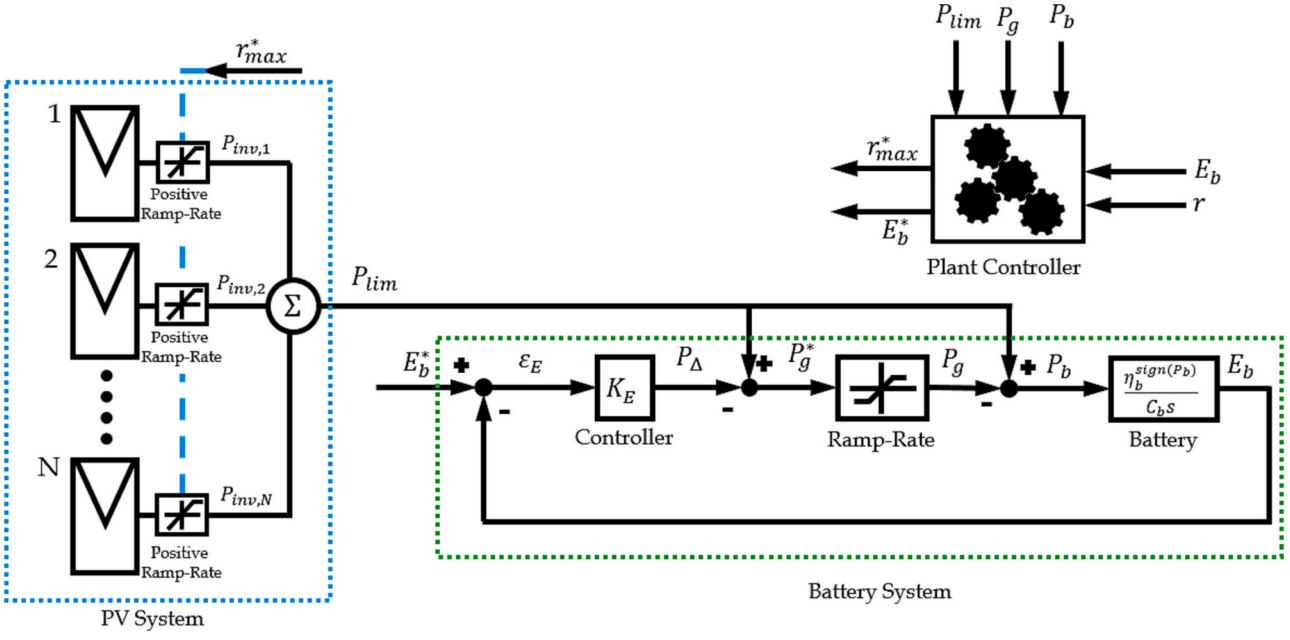

Fig. 6. Proposed control to regulate coordinately PV inverters and battery system.

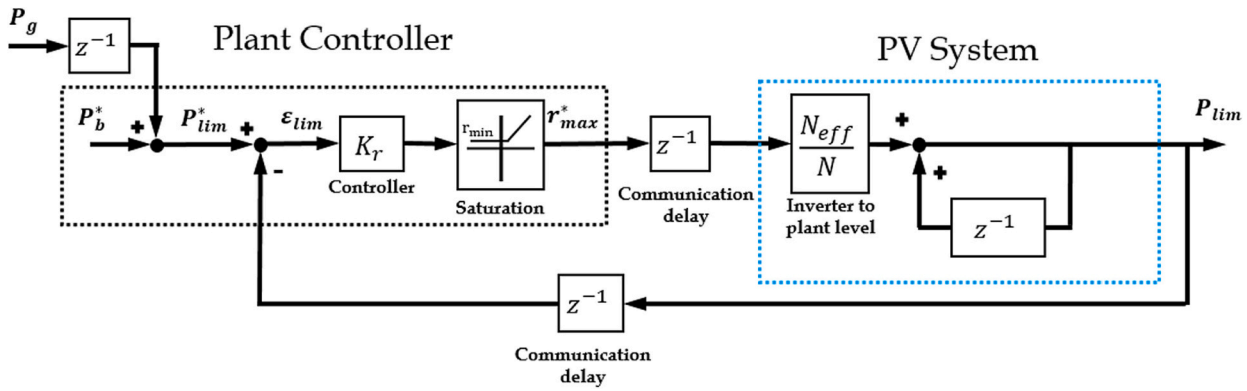

Fig. 7. Smart Limitation Loop (SLL) during upward fluctuations.

the 5-second sampling time of our data.

5.1.1. SLL tuning

The open loop of SLL (Fig. 7), without saturation, is:

$$G = \frac{P_{lim}}{P_{lim}^*} = K_r \frac{N_{eff}}{N} z^{-2} \frac{1}{1 - z^{-1}} \tag{8}$$

which comprises a variable DC gain ($K_r N_{eff}/N$) and an integrator with double delay ($z^{-2}/(1 - z^{-1})$. Its Bode plot with unity proportional gain ($K_r = 1$) and the extreme conditions of N_{eff} are shown in Fig. 8.

The DC gain displaces the magnitude plot of (8) in the y-direction, which modifies the cutoff frequency. From Fig. 8, it can be concluded that $K_r < 1$, given that if $K_r N_{eff}/N = 1$ and $K_r = 1$ the phase margin of (8) would be zero and the system would be unstable. The reader should remember that the value N_{eff}/N can vary between 1 and $1/N$, which means that the maximum cutoff frequency is determined by K_r and that the maximum instability condition is produced when $N_{eff}/N = 1$; in any other condition the total gain would be smaller and the system would be more stable.

Using a proportionality relationship, the desired cutoff frequency (ω_c) and the required gain (K_r) can be related to the known SLL's cutoff frequency with unity gain ($\omega_c' \approx T^{-1}$, see Fig. 8):

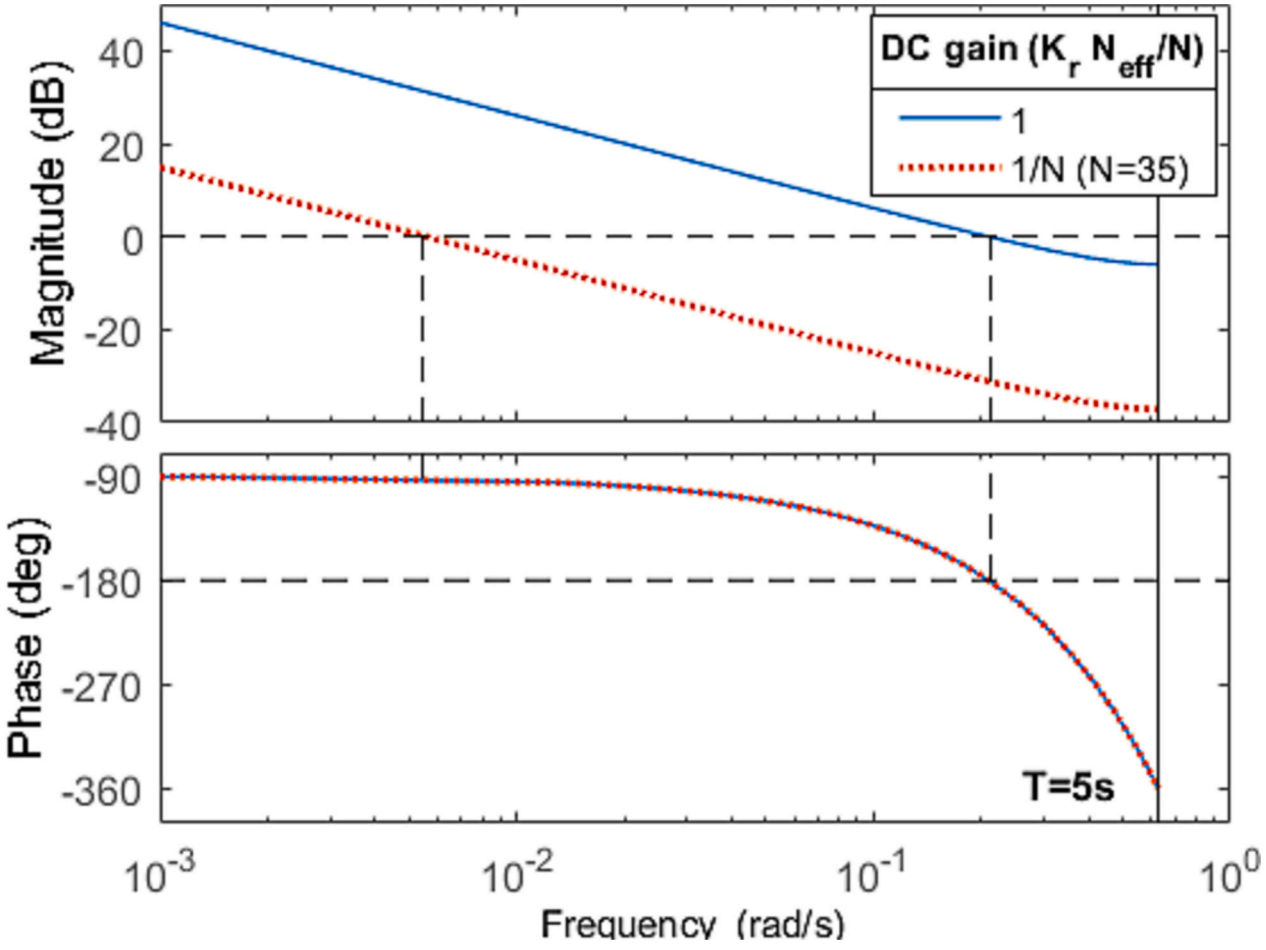

Fig. 8. Bode plot of the proposed loop to coordinate PV plant inverters (Fig. 7).

$$\frac{log\omega_c - log\omega_c^{'}}{-20logK_r} = -\frac{1}{20} \rightarrow log\omega_c = logK_r + log\omega_c^{'} \rightarrow \omega_c = K_r\omega_c^{'} \approx \frac{K_r}{T} \quad (9)$$

therefore, the phase margin (PM) would be:

$$PM \approx 180 - arg[G(Kr/T)] \quad (10)$$

From (9) and (10), an adequate value of the proportional gain is $K_r = 0.5$, which would produce a maximum cutoff frequency close to 0.1 rad/s and a phase margin of 46° (with a 5-second sampling time).

5.2. Implementation of strategies

Fig. 9 shows the schematic performance of the strategies presented in [26,27] (hereinafter Strategy 1 and Strategy 2, respectively) and a novel *smart coordinated inverter-limitation* (SCIL) which was developed to ensure a well-limited charging power and a considerable reduction in the limitation losses, commonly associated with inverter limitation-based strategies. SLL is able to implement all of them by applying minor modifications, i.e. by choosing the values of P_b^* and r_{min}.

5.2.1. Benchmark strategies

The reader must remember that strategies 1 and 2 apply similar battery control loops (see Fig. 6) with identical reference ($E_b^* = 100\%$) [26,27], but differ in the way in which the plant limitation is performed, i.e. with regard to the trajectory of P_{lim} during fluctuations (see Fig. 9 (a–b)).

To implement Strategy 1, P_b^* must be equal to P_Δ, the value of the proportional action of the loop of the Battery System (see Fig. 6). Finally, in order to obtain, at least, the same performance of Strategy 0, r_{min} takes the same value as the ramp-rate restriction (r). Its performance in the same conditions as Strategy 0 in Fig. 4 is shown in Fig. 10, which include r_{max}^* as is requested by SLL and, as a comparison, P_{lim} of Strategy 0 (yellow dashed line).

Looking at Fig. 10 there is an evident improvement achieved with the coordination allowed by SLL, first of all because there would no longer be any curtailment if P_g is higher than P_{lim} and no battery discharge would be extended in a counterproductive way (compare Fig. 10(b) and Fig. 4(b)). In addition, in Fig. 10(a) it can clearly be appreciated that when some inverters suffer sudden drops, SLL compensates them by increasing r_{max}^*, particularly after 12:46. For the entire day, the curtailment losses incurred by Strategy 1 would be 20.5 and 6.1, for ramp-rate restrictions of 2 and 10 %/min, respectively.

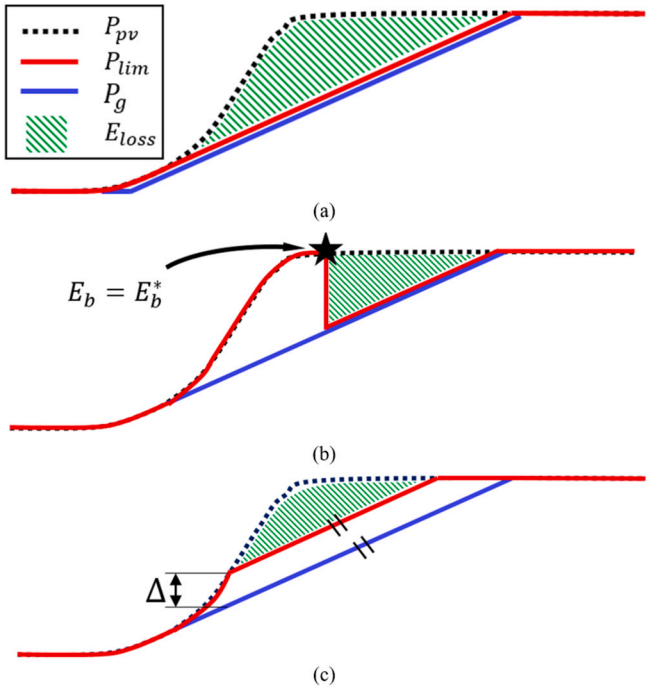

Fig. 9. Schematic behavior of strategies with coordinated inverters. (a) Strategy 1, (b) Strategy 2 and (c) Smart Coordinated Inverter Limitation (SCIL).

In Strategy 2, the inverters are not limited until the battery is at its setpoint; in practice, it should be done before $E_b^* = 100$ %, given that the required sharp P_{lim} reduction can be fast but not instantaneous (see Fig. 11(a)). This can be achieved if P_b^* is defined as a function of E_b, for example through a look-up table. P_b^* takes a high value, e.g. 1 pu, when the battery is far from full charge, which would avoid any limitation, and must decrease rapidly to zero when the battery approaches its reference. To produce the sharp reduction and avoid any further charge, the parameter of the saturation block (r_{min}, see Fig. 7) must be negative, for this strategy r_{mim} was set to $-3r$. A demonstration of the implementation of Strategy 2 can be seen in Fig. 11, showing the same fluctuation cases used for Strategy 0 (Fig. 4) and Strategy 1 (Fig. 10).

It is clear how the limitation problems highlighted in Fig. 4 are resolved: no discharge prolongation is produced in Fig. 11(b) and in both Fig. 11(a–b) P_{lim} is always equal to or higher than that of Strategy 0 (yellow-dashed line). In fact, no limitation is performed in Fig. 11(b) and very little in Fig. 11(a), outperforming not only Strategy 0 but also Strategy 1. For the entire day, Strategy 2 would induce limitation losses of 12.3 and 2.9 %, for $r = 2$ %/min and $r = 10$ %/min, respectively.

Fig. 11(a) demonstrates the notable performance of SLL to produce the desired operating plant condition (P_{lim}), in particular, the requested severe P_{lim} reduction just after 12:44. It is evident how the changes in r_{max}^* produce the P_{lim} drop and then its constant growth, limited to r.

5.2.2. Proposed control strategy: Smart Coordinated Inverter Limitation (SCIL)

The proposed strategy (SCIL) is based on a coherent definition of the references of the two control loops present in the system (E_b^* and P_b^*, see Fig. 6 and Fig. 7). Firstly, the SLL reference (P_b^*) is set to a proper value Δ (see Fig. 9(c)), which enables the Plant Controller to limit all battery charges to this value, avoiding high charging power/currents (triggers of accelerated degradation processes [32–34]), as Strategy 2, and excessive energy curtailments, as Strategy 1 and particularly Strategy 0. This can be done by means of a look-up table as a function of the stored energy, as in Fig. 12 (see below). The selection of the proper definition of P_b^* is out of the scope of this study, but it should depend on the chemistry of the battery and especially on the evolution of its equivalent internal series resistance and the open circuit voltage with SOC and temperature.

Secondly, the way in which the previous strategies (0, 1 and 2) define E_b^* makes them unnecessarily increase their limitation losses [29], we would therefore propose a variable reference that avoids charging at low irradiance conditions if no ramp-rate violation occurs. This would increase the margin of energy recovery when the next ramp-up is smoothed. The Plant Controller continuously calculates the proper reference, using the worst-case fluctuation model (1)–(3), and then transmits it to the Battery Subsystem. If ΔP_{max} is replaced by P_{lim} in (3), which assumes a total power reduction that disregards diffuse radiation, the required stored energy to mitigate the maximum instantaneous power drop (E_{drop}) that could happen can be estimated:

$$E_{drop}(k) = P_{lim}(k-1)\left(\frac{P_{lim(k-1)}}{2r} - \tau\right) \quad (11)$$

with the use of (11), it can be determined whether the stored energy (E_b) is sufficient to cover the eventual drop, therefore, a proper reference can be obtained:

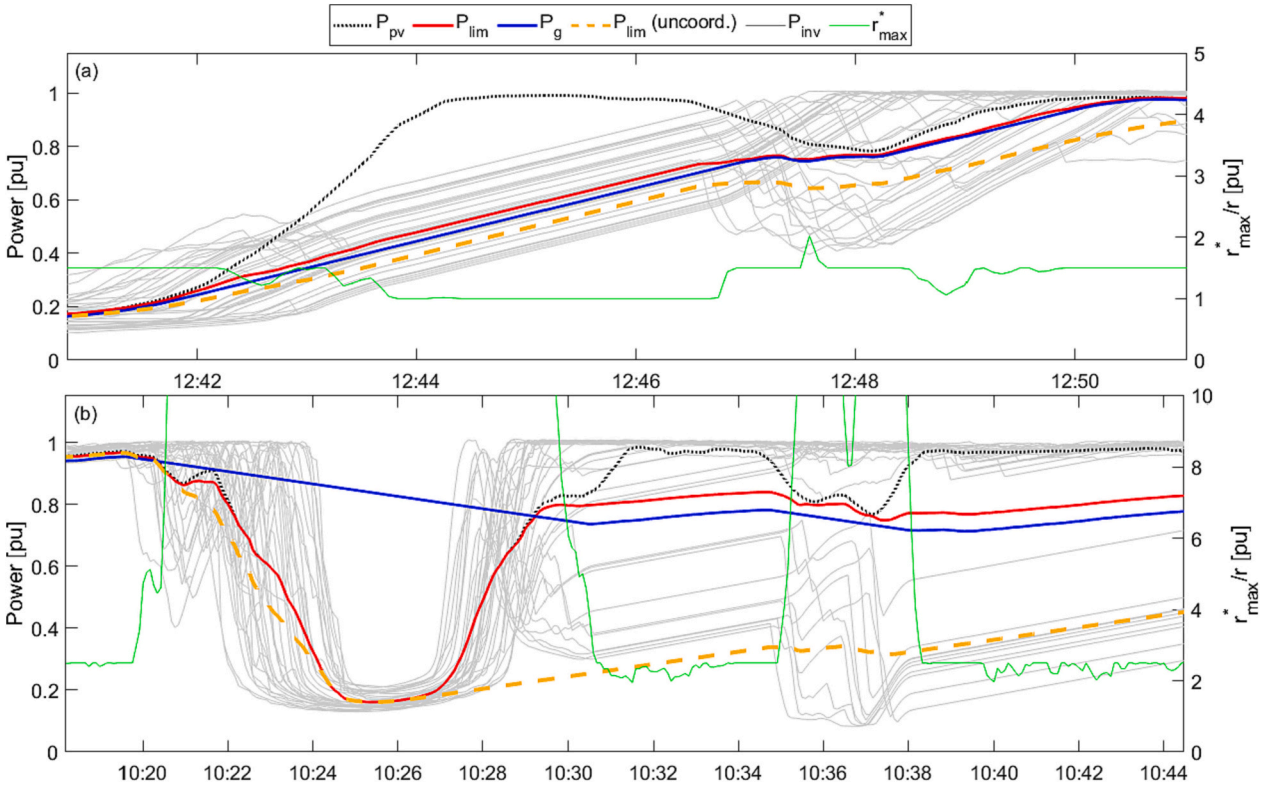

Fig. 10. Strategy 1 performance during portions of 28th of January. (a) $r = 10$ %/min and (b) $r = 2$ %/min. Available PV power P_{pv} (black-dotted), limited PV power P_{lim} (red), injected power P_g (blue), uncoordinated P_{lim} (yellow-dashed), inverters' production P_{inv} (gray) and ramp limitation r^*_{max} (green). (For interpretation of the references to colour in this figure legend, the reader is referred to the web version of this article.)

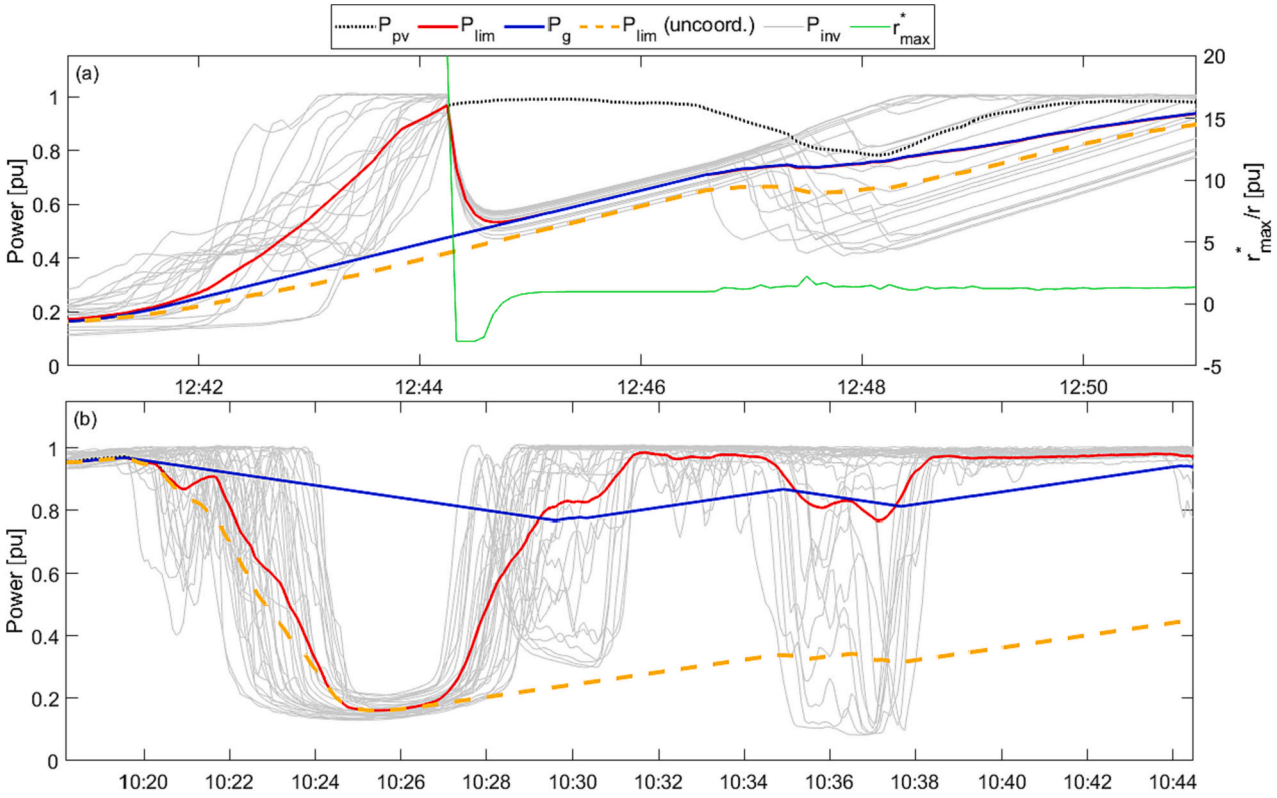

Fig. 11. Strategy 2 performance during portions of 28th of January. (a) r = 10 %/min and (b) r = 2 %/min. Available PV power P_{pv} (black-dotted), limited PV power P_{lim} (red), injected power P_g (blue), uncoordinated P_{lim} (yellow-dashed), inverters' production P_{inv} (gray) and ramp limitation r^*_{max} (green). In (b), r^*_{max} was ommited due to the absence of limitation. (For interpretation of the references to colour in this figure legend, the reader is referred to the web version of this article.)

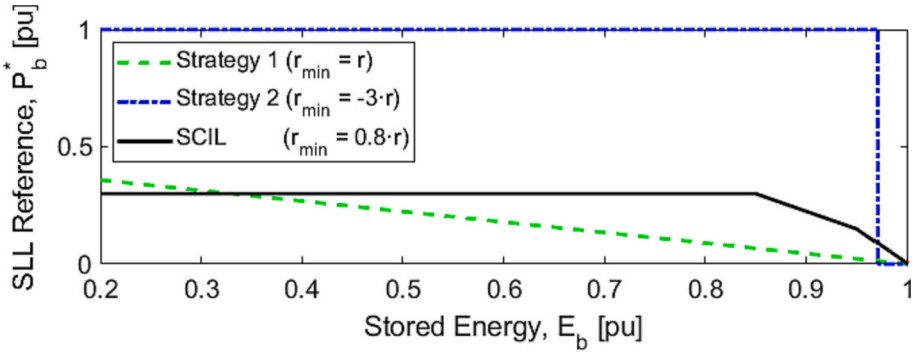

Fig. 12. Sets of control parameters to implement inverter limitation based strategies. For all cases, $K_E/C_b = 1\left[h^{-1}\right]$ and $K_r = 0.5$.

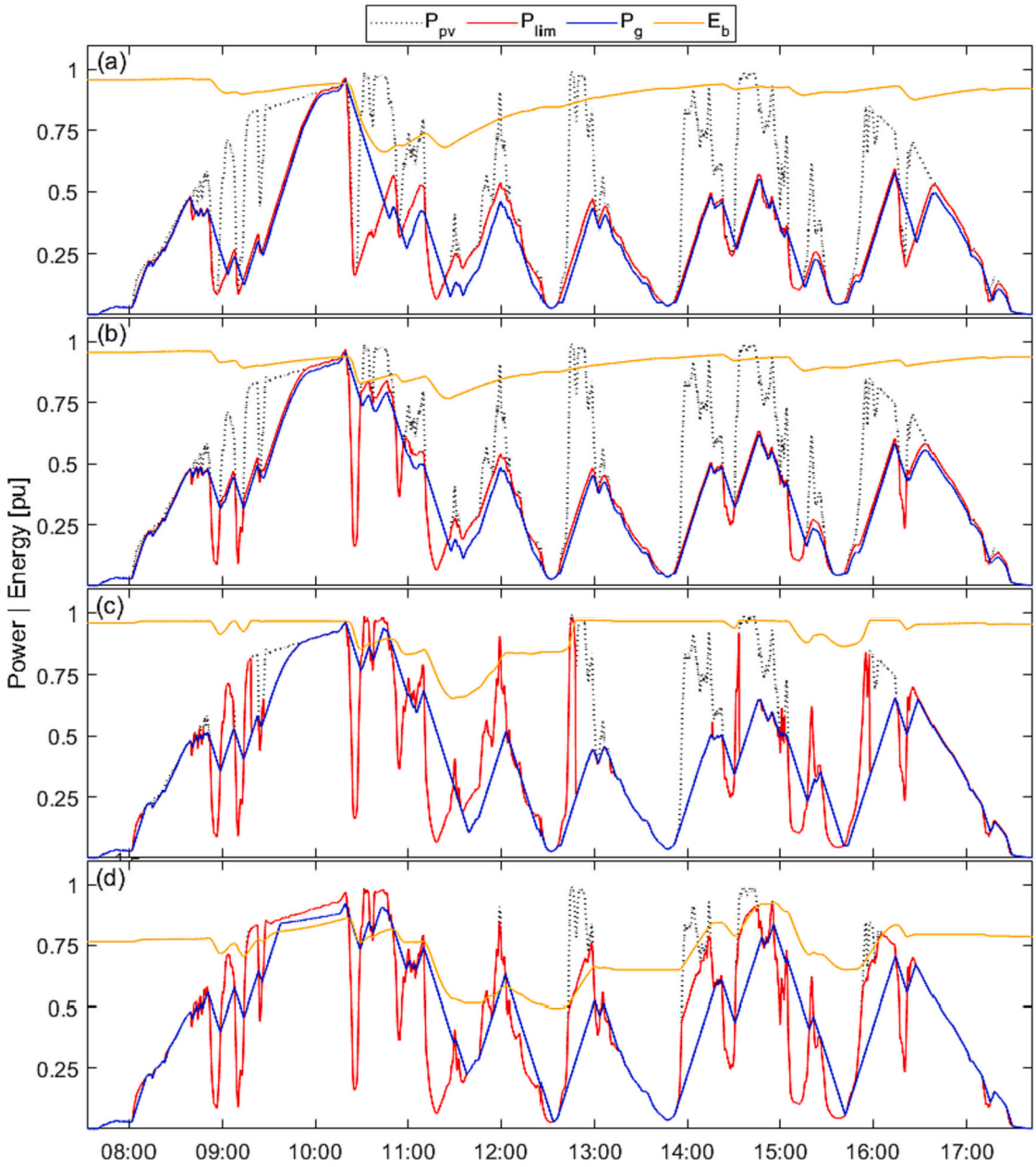

Fig. 13. Performance of strategies with coordinated inverters using SLL during 28th of January and zoom view with individual inverters ($r = 2$ %/min). (a) Strategy 0, (b) Strategy1, (c) Strategy 2 (d) SCIL. Available PV power P_{pv} (black-dotted), limited PV power P_{lim} (red), injected power P_g (blue), stored energy E_b (yellow). (For interpretation of the references to colour in this figure legend, the reader is referred to the web version of this article.)

$$\begin{aligned} &\text{if } E_{min} + E_{drop} > E_b(k-1) \\ &\quad E_b^*(k) = E_{min} + E_{drop} \\ &\text{else} \\ &\quad E_b^*(k) = E_b(k-1) \end{aligned} \tag{12}$$

where E_{min} is the minimum permitted condition. Based on (4), $E_{min} = 20$ %.

Finally, in order to avoid the possible full charge or discharge of the battery due to small steady-state fluctuations, a safety margin (E_s) limits the maximum and minimum value of E_b^*:

$$E_{min} + E_s < E_b^* < E_{max} - E_s \tag{13}$$

where $E_{max} = 100\%$. In this study E_s was set at 3 %.

The simulated performance of SCIL is shown in Fig. 13(d) (see below).

6. Simulation results

All the strategies based on inverter-limitation (0–2 and SCIL) were simulated using 1-year data from a real multi-megawatt PV plant (see Fig. 1). The simulations requiring inverter coordination were performed using the flexibility of SLL. Following the tuning rule suggested in [35], K_E was set to meet $K_E/C_b = 1\left[h^{-1}\right]$. According to SLL tuning, in the case of coordinated inverters $K_r = 0.5$. The remaining control parameters used to simulate the strategies (r_{min} and P_b^*) are summarized in Fig. 12.

The strategies were evaluated in the short-term (the performance in a day with severe power fluctuations) and in the long-term (for different ramp-rate restrictions). The analysis of the short term makes it possible to justify the results of the long term.

Under identical ramp-rate constraints, the battery capacity (C_b) was set for all strategies following (4). The values of the simulated capacities are shown in Table 1, both in absolute terms (in MWh) and relative to the plant nameplate capacity (in minutes of storage). As can be seen, the required storage increases dramatically as the ramp-rate limitation becomes more restrictive. The initial condition ($E_b(0)$) for all the strategies was the same (fully charged).

The constraints applied during simulation are the set of Eqs. (14)–(18), expressed in pu: (14) ensures the ramp-rate limitation; (15) and (16) represent the conservation of energy; (17) guarantees that P_g will not be neither negative (charge from the grid), nor higher than the plant rated power; and (18) represents the battery operation limits.

$$|\Delta Pg| \leq r \tag{14}$$

$$P_g = P_{lim} - P_b \tag{15}$$

$$P_{lim}(k) = \sum P_{inv,i}(k) \leq P_{pv}(k) \tag{16}$$

$$min\{0.1, P_{pv}(k)\} \leq P_g(k) \leq 1 \tag{17}$$

$$0.2 < E_b(k) < 1 \tag{18}$$

6.1. Short-term simulation: a day with severe power fluctuations

As an illustration, one highly variable day of the entire simulated year (28th of January) is shown for all the strategies and the same ramp-rate restriction ($r = 2$ %/min). Fig. 13 shows the entire day: Strategy 0 (Fig. 13(a)), Strategy 1 (Fig. 13(b)), Strategy 2 (Fig. 13(c)) and SCIL (Fig. 13(d)).

Even though the different strategies can effectively limit the ramp-rate of P_g to the same value, with an identical storage amount, the use of one or another has different implications from the point of view of the battery stress factors and energy production.

In the first case, for fixed setpoint $E_b^* = 100\%$ strategies (0–2) the battery would operate at higher charge levels, on this particular day, it would operate between its setpoint and 65 %, as can be seen in Fig. 13 (a–c) (which accelerates calendar degradation), while SCIL operates between 50 and 90 %. Furthermore, Strategy 2, the benchmark strategy with less losses, demands high power rates while charging (which increases cycling degradation), as can be seen in Fig. 13(c) after 12:45. In contrast, SCIL positively limits any charging power to the predefined value (see Fig. 12), which reduces the stress caused on the battery during the charging process.

On the other hand, by comparing the difference between (P_{lim}, red line) and the available power (P_{pv}, black dotted line), which defines the total limitation losses, it is clear that SCIL outperforms any of the previous strategies (see Fig. 13). For this particular day, SCIL limits 3.8 % of the available energy, a negligible value compared to the range of the remaining strategies (between 12.3 and 32 %, see Table 2). The reason behind the SCIL low losses is the fact that its design makes the strategy recover energy in all ramp-up events, while in contrast, the previous strategies and their almost absent energy recovery in the consecutive power surges after midday (see Fig. 13(a–c)). This is due to the fact that SCIL not only avoids any limitation produced by a lack of coordination, such as in strategies 1 and 2, but also due to the fact that it operates with a less charged battery; thanks to the variable setpoint (11)–(13) the battery can be used to store and recover energy in all power surges. In contrast, as strategies 0–2 tend to be charged for a longer period of time, they reduce the possibility of absorbing energy while smoothing power fluctuations.

The above can be easily corroborated in the progressive reduction of curtailment losses from Fig. 13(a) to (d). For example, the continuous disappearance of inverter limitation in the early morning (before 11:00) and the increase in energy recovery afterwards.

The results of Fig. 13 are presented Fig. 14 in a different way to evidence the link between two variables directly related to the charging stress (E_b and P_b), which are paired in a simultaneous basis. In other words, Fig. 14 shows the severity of the charge/discharge process and at what estimated SOC level they would occur. As can be seen, the strategies 0 and 1 have the lowest charging rates, but at high SOC levels (especially Strategy 0), and at the same time they are the ones that waste more energy. On the contrary, among the benchmark strategies, Strategy 2 (blue line) is the one that less energy curtails, but has high charging rates at high SOC levels (note the highlighted region).

SCIL represents a tradeoff between them: on the one hand, extremely low energy losses (see Table 2), and, on the other hand, limited charging rates (0.3 pu in the simulated scenarios, see Fig. 12). Additionally, given the variable E_b reference (11)–(13), it is clearly appreciated how the SOC levels at which the charges occur are lower than in the benchmark strategies, allowing low charging rates with intermediate SOC levels. Finally, thanks to the ability of SLL to limit the charge rate, the profile used for P_b^* (see Fig. 12), can be reduced to a lower constant value, such as 0.2 or 0.1 pu, to a further reduction of the charging stress (in exchange of higher curtailment losses), or even use more complex forms to set P_b^*, but, as previously said, this is beyond the scope of this work.

6.2. Long-term simulations: annual limitation losses

The trend observed on 28th of January is the same when the entire year is considered. Table 2 shows the comparison of the different

Table 2
Summary of energy curtailment losses for different inverter-limitation strategies ($r = 2\%/min$).

Strategy	Annual [%]	28th of January [%]
0	6.4	32
1	3.4	20.5
2	2.2	12.3
SCIL	0.28	3.8

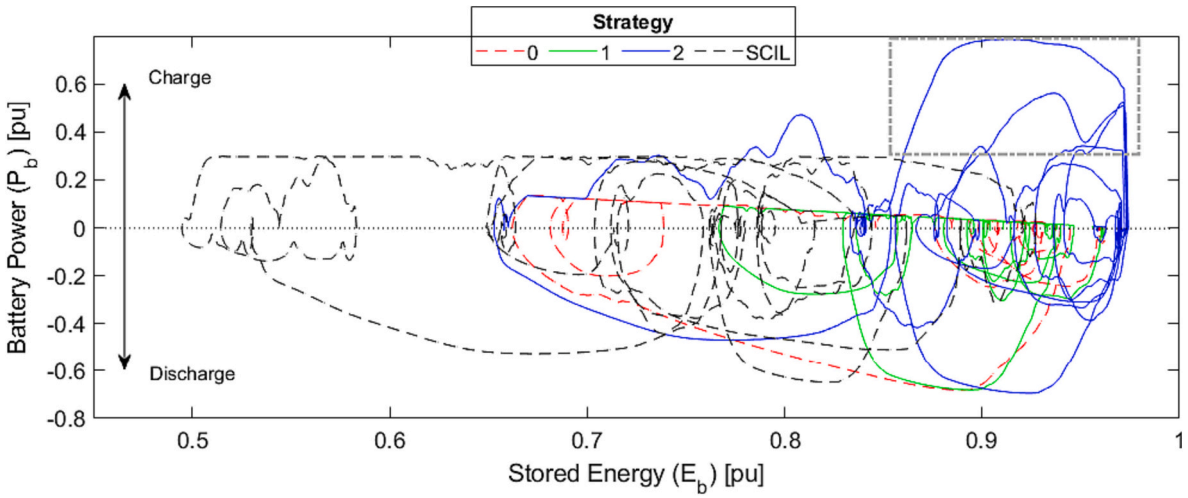

Fig. 14. Battery power (P_b) versus stored energy (E_b) during the 28th of January. Strategy 0 (red dashed), Strategy 1 (green), Strategy 2 (blue) and SCIL (black dashed). High SOC values coincide with high power/current charge rates in the region enclosed by the gray rectangle. (For interpretation of the references to colour in this figure legend, the reader is referred to the web version of this article.)

strategies. For each strategy, its annual limitation losses are lower than those of January 28th, given that the curtailment on clear days is very low or non-existent (and these days are a majority in the overall). However, the trend observed on January 28th is maintained: Strategy 0 shows very high losses, while SCIL presents negligible values (and strategies 1–2 would imply curtailment values closer to Strategy 0 than to SCIL). In fact, the annual limitation of SCIL (0.28 %) is an order of magnitude below the benchmark strategies (between 2.2 and 6.4 %).

The same performance can be observed if the limitation losses are calculated for different ramp-rate restrictions. The results can be seen in Fig. 15. As expected, all strategies exhibit lower production losses as the ramp-rate limit becomes less restrictive, given that inverter curtailments become less frequent as dispersion smoothing becomes more effective [30,31].

Regardless of the required ramp-rate smoothing, the relative positions of the strategies in Table 2 do not change: the uncoordinated limitation (Strategy 0) wastes more energy than any other smoothing method, while SCIL produces insignificant curtailment losses over the full range of ramp-rate restrictions (0.64 % curtailment at a ramp restriction of 1 %/min and 0.05 % at 10 %/min).

7. Conclusion

This study addresses the implementation of ramp-rate limiting strategies in multi-megawatt PV plants. Although different limiting strategies have been proposed in earlier investigations, no algorithm capable of regulating the combined power of the inverters has been presented, particularly in scenarios of severe power fluctuations when there is a large dispersion in the operating point of the different PV generators.

A control method has been presented to overcome this technical shortcoming. The method is based on the coordination between the control loop that governs the storage device and a new control loop implemented in the plant controller that regulates the overall operating point of the plant (called Smart Limitation Loop, SLL). The effectiveness and versatility of SLL have been demonstrated by correctly simulating the various inverter limitation strategies proposed to date. SLL is able to handle the 5-second sampling time in the system analyzed, a higher value than the communication delay in current PV facilities, which indicates that its implementation is feasible in real systems.

Furthermore, a novel strategy (called SCIL: Smart Coordinated Inverter Limitation) has been proposed. Taking account of the potential of SLL and a correct coordination with the battery controller, SCIL makes it possible to limit the battery charge power to any desired value and to keep it constant during any positive fluctuation (without violating the imposed ramp-rate limit). This makes the system to recover energy during any upward fluctuation and to reduce the limiting losses to negligible values (<1 % for any ramp limitation). As an example, for a

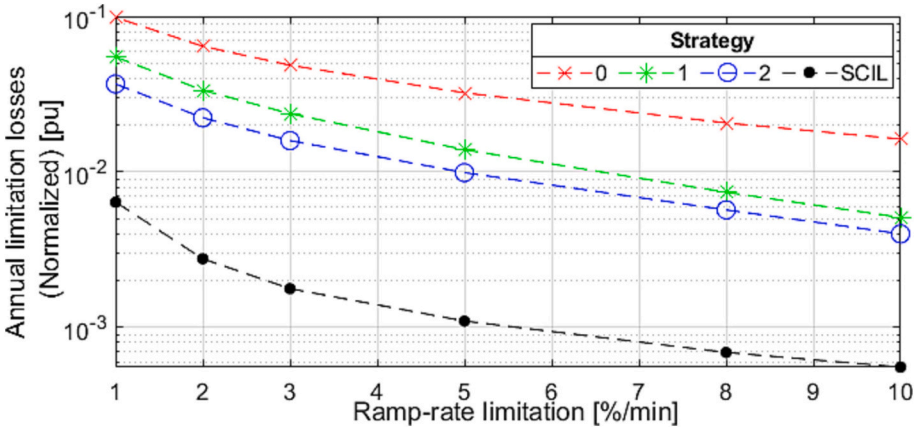

Fig. 15. Annual losses for different ramp-rate restrictions and inverter limitation-based strategies. Strategy 0 (red), Strategy 1 (green), Strategy 2 (blue) and SCIL (black). (For interpretation of the references to colour in this figure legend, the reader is referred to the web version of this article.)

ramp-rate restriction of 2 %/min, SCIL would waste 0.28 % of the available production, while different benchmark strategies would lose between 2.2 and 6.4 %. Finally, SCIL makes it possible to operate batteries in safer conditions: lower SOC levels and, as it is able to limit charge to any desired value, to reduce charge rates.

The value of SLL is not only limited to the implementation of battery-dependent strategies; its ability to control the operating point of the plant by modifying each of the inverters makes it a viable technique for implementing battery-less strategies, which, with the help of PV forecasting methods, proactively smooth out power fluctuations [36–39]. The synergies between these methods and SLL are an interesting topic of research that could have the capacity to minimize the effect of intermittency on the increasing number of large grid-connected PV installations.

CRediT authorship contribution statement

A. González-Moreno: Formal analysis, Writing – original draft, Conceptualization, Methodology, Visualization. **J. Marcos:** Conceptualization, Writing – review & editing, Supervision. **I. de la Parra:** Data curation. **L. Marroyo:** Conceptualization, Writing – review & editing, Supervision.

Declaration of competing interest

The authors declare that they have no known competing financial interests or personal relationships that could have appeared to influence the work reported in this paper.

Data availability

The data that has been used is confidential.

Acknowledgement

The authors would like to thank ACCIONA for authorizing measurements at its PV plants and for the helpful collaboration of its staff. Likewise, we would like to acknowledge the support of the Spanish State Research Agency (AEI) under grants PID2019111262RB-I00 and PID2019-110816RB-C21. Alejandro González-Moreno would like to thank the Universidad Pública de Navarra (UPNA) for its financial support. Open access funding provided by Universidad Pública de Navarra.

References

[1] C. Kost, S. Shammugam, V. Jülch, H.-T. Nguyen, T. Schlegl, Levelized Cost of Electricity- Renewable Energy Technologies, 2018.
[2] LAZARD, Lazard's Levelized Cost of Energy Analysis—Version 16.0, LAZARD, 2023.
[3] IRENA, Renewable Power Generation Costs in 2020, International Renewable Energy Agency, Abu Dhabi, 2021.
[4] IRENA, Renewable Energy Statistics 2021, International Renewable Energy Agency, Abu Dhabi, 2021.
[5] REN21, Renewables 2021: Global Status Report, REN21 Secretariat, Paris, 2022.
[6] D.S. Kumar, S. Maharjan, Albert, D. Srinivasan, Ramp-rate limiting strategies to alleviate the impact of PV power ramping on voltage fluctuations using energy storage systems, Sol. Energy 234 (2022) 377–386, https://doi.org/10.1016/j.solener.2022.01.059.
[7] S. Maharjan, D. Sampath Kumar, A.M. Khambadkone, Enhancing the voltage stability of distribution network during PV ramping conditions with variable speed drive loads, Appl. Energy 264 (2020), 114733, https://doi.org/10.1016/j.apenergy.2020.114733.
[8] A. Cabrera-Tobar, E. Bullich-Massagué, M. Aragüés-Peñalba, O. Gomis-Bellmunt, Review of advanced grid requirements for the integration of large scale photovoltaic power plants in the transmission system, Renew. Sust. Energ. Rev. 62 (2016) 971–987, https://doi.org/10.1016/j.rser.2016.05.044.
[9] G.S. Seck, V. Krakowski, E. Assoumou, N. Maïzi, V. Mazauric, Embedding power system's reliability within a long-term Energy System Optimization Model: linking high renewable energy integration and future grid stability for France by 2050, Appl. Energy 257 (2020), 114037, https://doi.org/10.1016/j.apenergy.2019.114037.
[10] PREPA, Puerto Rico Electric Power Authority Minimum Technical Requirements for Photovoltaic Generation (PV) Projects, Puerto Rico Electric Power Authority, 2012.
[11] V. Gevorgian, S. Booth, Review of PREPA Technical Requirements for Interconnecting Wind and Solar Generation, 2013, https://doi.org/10.2172/1260328.
[12] State Grid Corporation of China, Technical requirements for connecting photovoltaic power station to power system (GB/T 19964-2012). https://www.chinesestandard.net/PDF.aspx/GBT19964-2012, 2012.
[13] ENERGINET, Technical regulation 3.2.2 for PV power plants above 11 kW. https://en.energinet.dk/Electricity/Rules-and-Regulations/Regulations-for-grid-connection, 2019 (accessed September 18, 2020).
[14] AEMC, National Electricity Rules Version 150, Australian Energy Market Commission, Australia, 2019. https://www.aemc.gov.au/regulation/energy-rules/national-electricity-rules/current.
[15] NERSA, Grid Connection Code for Renewable Power Plants (RPPs) Connected to the Electricity Transmission System (TS) or the Distribution System (DS) in South Africa. Version 3.0, National Energy Regulator of South Africa, South Africa, 2019. https://www.nersa.org.za/electricity-overview/electricity-grid-code/.
[16] S. Sukumar, M. Marsadek, K.R. Agileswari, H. Mokhlis, Ramp-rate control smoothing methods to control output power fluctuations from solar photovoltaic (PV) sources—a review, J. Energy Storage 20 (2018) 218–229, https://doi.org/10.1016/j.est.2018.09.013.
[17] R. Perez, T. Hoff, J. Dise, D. Chalmers, S. Kivalov, The cost of mitigating short-term PV output variability, Energy Procedia 57 (2014) 755–762, https://doi.org/10.1016/j.egypro.2014.10.283.
[18] M.J.E. Alam, K.M. Muttaqi, D. Sutanto, A novel approach for ramp-rate control of solar PV using energy storage to mitigate output fluctuations caused by cloud passing, IEEE Trans. Energy Convers. 29 (2014) 507–518, https://doi.org/10.1109/TEC.2014.2304951.
[19] R. Kini, D. Raker, T. Stuart, R. Ellingson, M. Heben, R. Khanna, Mitigation of PV variability using adaptive moving average control, IEEE Trans. Sustain. Energy 11 (4) (2019) 2252–2262, https://doi.org/10.1109/TSTE.2019.2953643.
[20] C. Jamroen, E. Usaratniwart, S. Sirisukprasert, PV power smoothing strategy based on HELES using energy storage system application: a simulation analysis in microgrids, IET Renew. Power Gener. 13 (2019) 2298–2308, https://doi.org/10.1049/iet-rpg.2018.6165.
[21] J. Marcos, I. de la Parra, M. García, L. Marroyo, Control strategies to smooth short-term power fluctuations in large photovoltaic plants using battery storage systems, Energies 7 (2014) 6593–6619, https://doi.org/10.3390/en7106593.
[22] J. Marcos, O. Storkël, L. Marroyo, M. Garcia, E. Lorenzo, Storage requirements for PV power ramp-rate control, Sol. Energy 99 (2014) 28–35, https://doi.org/10.1016/j.solener.2013.10.037.
[23] I. de la Parra, J. Marcos, M. García, L. Marroyo, Control strategies to use the minimum energy storage requirement for PV power ramp-rate control, Sol. Energy 111 (2015) 332–343, https://doi.org/10.1016/j.solener.2014.10.038.
[24] G. Chandra Mahato, S. Ranjan Biswal, T. Roy Choudhury, B. Nayak, S. Bikash Santra, Review of active power control techniques considering the impact of MPPT and FPPT during high PV penetration, Sol. Energy 251 (2023) 404–419, https://doi.org/10.1016/j.solener.2023.01.035.
[25] A. Sangwongwanich, Y. Yang, F. Blaabjerg, A cost-effective power ramp-rate control strategy for single-phase two-stage grid-connected photovoltaic systems, in: 2016 IEEE Energy Conversion Congress and Exposition (ECCE), IEEE, Milwaukee, WI, USA, 2016, pp. 1–7, https://doi.org/10.1109/ECCE.2016.7854671.
[26] I. de la Parra, J. Marcos, M. García, L. Marroyo, Improvement of a control strategy for PV power ramp-rate limitation using the inverters: reduction of the associated energy losses, Sol. Energy 127 (2016) 262–268, https://doi.org/10.1016/j.solener.2016.01.032.
[27] A. Makibar, L. Narvarte, E. Lorenzo, Contributions to the size reduction of a battery used for PV power ramp rate control, Sol. Energy 230 (2021) 435–448, https://doi.org/10.1016/j.solener.2021.10.047.
[28] I. de la Parra, J. Marcos, M. García, L. Marroyo, Dealing with the implementation of ramp-rate control strategies – challenges and solutions to enable PV plants with energy storage systems to operate correctly, Sol. Energy 169 (2018) 242–248, https://doi.org/10.1016/j.solener.2018.04.054.
[29] A. Gonzalez-Moreno, J. Marcos, I. De La Parra, L. Marroyo, Inverter-based PV ramp-rate limitation strategies: minimizing energy losses, in: 2022 IEEE 7th International Energy Conference (ENERGYCON), IEEE, Riga, Latvia, 2022, pp. 1–6, https://doi.org/10.1109/ENERGYCON53164.2022.9830218.
[30] A. Murata, H. Yamaguchi, K. Otani, A method of estimating the output fluctuation of many photovoltaic power generation systems dispersed in a wide area, Electr. Eng. Jpn. 166 (2009) 9–19, https://doi.org/10.1002/eej.20723.
[31] J. Marcos, L. Marroyo, E. Lorenzo, D. Alvira, E. Izco, From irradiance to output power fluctuations: the PV plant as a low pass filter, Prog. Photovolt. Res. Appl. 19 (2011) 505–510, https://doi.org/10.1002/pip.1063.
[32] M. Ecker, N. Nieto, S. Käbitz, J. Schmalstieg, H. Blanke, A. Warnecke, D.U. Sauer, Calendar and cycle life study of Li(NiMnCo)O2-based 18650 lithium-ion batteries, J. Power Sources 248 (2014) 839–851, https://doi.org/10.1016/j.jpowsour.2013.09.143.
[33] J. Schmalstieg, S. Käbitz, M. Ecker, D.U. Sauer, A holistic aging model for Li (NiMnCo)O2 based 18650 lithium-ion batteries, J. Power Sources 257 (2014) 325–334, https://doi.org/10.1016/j.jpowsour.2014.02.012.
[34] I. Baghdadi, O. Briat, J.-Y. Delétage, P. Gyan, J.-M. Vinassa, Lithium battery aging model based on Dakin's degradation approach, J. Power Sources 325 (2016) 273–285, https://doi.org/10.1016/j.jpowsour.2016.06.036.

[35] A. González-Moreno, J. Marcos, I. de la Parra, L. Marroyo, Influence of control in cycling degradation when batteries perform PV ramp-rate control, IEEE Trans. Ind. Appl. (2023) 1–9, https://doi.org/10.1109/TIA.2023.3260810.
[36] X. Chen, X. Xu, J. Wang, L. Fang, Y. Du, E.G. Lim, J. Ma, Robust proactive power smoothing control of PV systems based on deep reinforcement learning, IEEE Trans. Sustain. Energy (2023) 1–14, https://doi.org/10.1109/TSTE.2023.3239852.
[37] M. Saleh, L. Meek, M.A.S. Masoum, M. Abshar, Battery-less short-term smoothing of photovoltaic generation using sky camera, IEEE Trans. Ind. Inform. 14 (2018) 403–414, https://doi.org/10.1109/TII.2017.2767038.
[38] H. Wen, Y. Du, X. Chen, E. Lim, H. Wen, L. Jiang, W. Xiang, Deep learning based multistep solar forecasting for PV ramp-rate control using sky images, IEEE Trans. Ind. Inform. 17 (2021) 1397–1406, https://doi.org/10.1109/TII.2020.2987916.
[39] Q. Paletta, G. Arbod, J. Lasenby, Omnivision forecasting: combining satellite and sky images for improved deterministic and probabilistic intra-hour solar energy predictions, Appl. Energy 336 (2023), 120818, https://doi.org/10.1016/j.apenergy.2023.120818.